Photon number squeezing in repeated parametric downconversion with ancillary photon-number measurements

Boris L. Glebov,[1,*] Jingyun Fan,[2,3] and A. Migdall[1,2]

[1]*Joint Quantum Institute, Univ. of Maryland, College Park, MD 20742, USA*
[2]*National Institute of Standards and Technology, Gaithersburg, MD 20899, USA*
[3]*jfan @nist.gov*
[*]*boris.glebov@nist.gov*

Abstract: We present a realistic numerical simulation of a source of number-squeezed photon states employing a cavity-based parametric downconversion (PDC) process. A cavity containing the PDC medium is pumped repeatedly. The cavity recycles only one of the PDC output modes, allowing it to be amplified with each subsequent pump pulse. A photon number resolved (PNR) measurement is made on the other PDC output mode following each pump pulse. Once the PNR measurements indicate that the target number of photons has accumulated in the cavity, the pumping is stopped and the resulting photon state is released. The photon number uncertainty in the resulting state is ~3 dB below that of a mean-equivalent coherent state and furthermore the probability of generating the target photon number is similarly increased.

OCIS codes: (270.0270) Quantum optics; (270.4180) Multiphoton processes; (270.6570) Squeezed states.

References and links

1. C. M. Caves, "Quantum-mechanical noise in an interferometer," Phys. Rev. D Part. Fields **23**(8), 1693–1708 (1981).
2. V. Giovannetti, S. Lloyd, and L. Maccone, "Quantum metrology," Phys. Rev. Lett. **96**(1), 010401 (2006).
3. T. Nagata, R. Okamoto, J. L. O'brien, K. Sasaki, and S. Takeuchi, "Beating the standard quantum limit with four-entangled photons," Science **316**(5825), 726–729 (2007).
4. A. N. Boto, P. Kok, D. S. Abrams, S. L. Braunstein, C. P. Williams, and J. P. Dowling, "Quantum interferometric optical lithography: Exploiting entanglement to beat the diffraction limit," Phys. Rev. Lett. **85**(13), 2733–2736 (2000).
5. P. Kok, A. N. Boto, D. S. Abrams, C. P. Williams, S. L. Braunstein, and J. P. Dowling, "Quantum-interferometric optical lithography: toward arbitrary two-dimensional patterns," Phys. Rev. A **63**(6), 063407 (2001).
6. M. D'Angelo, M. V. Chekhova, and Y. Shih, "Two-photon diffraction and quantum lithography," Phys. Rev. Lett. **87**(1), 013602 (2001).
7. A. Kuzmich and L. Mandel, "Sub-shot-noise interferometric measurements with two-photon states," Quantum Semiclass. Opt. B **10**(3), 493–500 (1998).
8. I. Afek, O. Ambar, and Y. Silberberg, "High-NOON states by mixing quantum and classical light," Science **328**(5980), 879–881 (2010).
9. L. K. Shalm, R. B. A. Adamson, and A. M. Steinberg, "Squeezing and over-squeezing of triphotons," Nature **457**(7225), 67–70 (2009).
10. K. J. Resch, K. L. Pregnell, R. Prevedel, A. Gilchrist, G. J. Pryde, J. L. O'Brien, and A. G. White, "Time-reversal and super-resolving phase measurements," Phys. Rev. Lett. **98**(22), 223601 (2007).
11. B. G. Christensen, K. T. McCusker, J. B. Altepeter, B. Calkins, T. Gerrits, A. E. Lita, A. Miller, L. K. Shalm, Y. Zhang, S. W. Nam, N. Brunner, C. C. W. Lim, N. Gisin, and P. G. Kwiat, "Detection-loophole-free test of quantum nonlocality, and applications," Phys. Rev. Lett. **111**(13), 130406 (2013).
12. M. Giustina, A. Mech, S. Ramelow, B. Wittmann, J. Kofler, J. Beyer, A. E. Lita, B. Calkins, T. Gerrits, S. W. Nam, R. Ursin, and A. Zeilinger, "Bell violation using entangled photons without the fair-sampling assumption," Nature **497**(7448), 227–230 (2013).

#206059 - $15.00 USD Received 28 Mar 2014; revised 29 May 2014; accepted 2 Jun 2014; published 15 Aug 2014

13. M. Da Cunha Pereira, F. E. Becerra, B. L. Glebov, J. Fan, S. W. Nam, and A. Migdall, "Demonstrating highly symmetric single-mode, single-photon heralding efficiency in spontaneous parametric downconversion," Opt. Lett. **38**(10), 1609–1611 (2013).
14. A. E. Lita, A. J. Miller, and S. W. Nam, "Counting near-infrared single-photons with 95% efficiency," Opt. Express **16**(5), 3032–3040 (2008).
15. F. Marsili, V. B. Verma, J. A. Stern, S. Harrington, A. E. Lita, T. Gerrits, I. Vayshenker, B. Baek, M. D. Shaw, R. Mirin, and S. W. Nam, "Detecting single infrared photons with 93% system efficiency," arXiv.org 1209.5774, 1–16 (2012).
16. Q. Zhao, A. McCaughan, F. Bellei, F. Najafi, D. De Fazio, A. Dane, Y. Ivry, and K. K. Berggren, "Superconducting –nanowire single-photon-detector linear array," Appl. Phys. Lett. **103**(14), 142602 (2013).
17. P. G. Kwiat, K. Mattle, H. Weinfurter, A. Zeilinger, A. V. Sergienko, and Y. Shih, "New high-intensity source of polarization-entangled photon pairs," Phys. Rev. Lett. **75**(24), 4337–4341 (1995).
18. P. J. Thomas, M. H. Dunn, D. J. M. Stothard, D. A. Walsh, and C. J. Chunnilall, "A pump enhanced source of telecom-band correlated photon pairs," J. Mod. Opt. **58**(8), 631–639 (2011).
19. L. Mandel and E. Wolf, *Optical Coherence and Quantum Optics* (Cambridge, Cambridge University, 1995).
20. P. G. Evans, R. S. Bennink, W. P. Grice, T. S. Humble, and J. Schaake, "Bright source of spectrally uncorrelated polarization-entangled photons with nearly single-mode emission," Phys. Rev. Lett. **105**(25), 253601 (2010).
21. K. T. McCusker and P. G. Kwiat, "Efficient optical quantum state engineering," Phys. Rev. Lett. **103**(16), 163602 (2009).
22. H. Zhang, X. Jin, J. Yang, H. Dai, S. Yang, T. Zhao, J. Rui, Y. He, X. Jiang, F. Yang, G. Pan, Z. Yuan, Y. Deng, Z. Chen, X. Bao, S. Chen, B. Zhao, and J. Pan, "Preparation and storage of frequency-uncorrelated entangled photons from cavity-enhanced spontaneous parametric downconversion," Nat. Photon. **5**(10), 628–632 (2011).
23. X. S. Ma, S. Zotter, J. Kofler, T. Jennewein, and A. Zeilinger, "Experimental generation of single photons via active multiplexing," Phys. Rev. A **83**(4), 043814 (2011).

1. Introduction

Photon-number states, also known as photon Fock states, have a De Broglie wavelength of λ/N_{ph}, where N_{ph} is the number of photons in the Fock state, $|N_{\mathrm{ph}}\rangle$. They have wide applicability in quantum metrology [1–3], quantum lithography [4–6], quantum imaging, and other quantum-enhanced techniques [7,8]. For example, several experiments have demonstrated super-resolution in position and phase through the use of photon Fock states [9, 10]. The typical signature of this improvement is the observation of an N_{ph}-fold increase in interference fringes when using photon Fock states as the light source relative to using a coherent light source. These "proof-of-principle" experiments typically employ Fock states with $N_{\mathrm{ph}} = 2$ or 4. But even for these small-photon-number Fock states, the low production rates of these N-photon events significantly reduces the statistical quality of the experimental data, and losses in photon collection further complicate the scenario by converting the initial photon Fock state into a mixture of states. As a result, the ultimate benefit of the higher fringe frequency in determining the system parameter of interest, for example, resolution and sensitivity in phase or space measurement, is reduced.

Recent experiments have demonstrated significant improvement in photon collection and detection efficiencies, both approaching unity [11–13]. In particular, advanced detectors, such as transition-edge sensors and superconducting nanowire systems of near unity detection efficiencies [14–16] are capable of photon-number-resolving (PNR) detection, which provides an advantage in these measurement applications. In contrast to these advances, efficient, high-rate generation of high photon number Fock states remains the bottleneck for many meaningful applications.

A common means of producing few-photon states is via heralded spontaneous parametric downconversion (SPDC) [17, 18]. In this scheme, a pump laser beam incident onto a nonlinear medium ideally produces a two-mode squeezed vacuum state [19]. The two modes can be separated assuming some non-degeneracy between the modes (such as polarization, wavelength, or direction). Ideally, performing a PNR detection on one mode (the ancillary number measurement) projects the other mode into a specific Fock state. The limitations of using this simple SPDC scheme to produce a specific Fock state are three-fold. First, free-space SPDC has very low efficiency in wavelength conversion. (We estimated a mean photon number $\mu = 1$ with a 10 nJ pump pulse in a SPDC process based on Ref [20].).) Second,

#206059 - $15.00 USD Received 28 Mar 2014; revised 29 May 2014; accepted 2 Jun 2014; published 15 Aug 2014

SPDC is inherently probabilistic, i.e., the photon Fock states produced via SPDC follows a Bose-Einstein distribution, which has a standard deviation of $\sigma_{\text{th}} = \sqrt{\mu^2 + \mu}$, which is wider than that of a Poisson distribution ($\sigma_{\text{P}} = \sqrt{\mu}$). Both this probabilistic nature and the high variance limit the rate of successful production of a desired photon Fock state. Furthermore, free space SPDC is ordinarily a multi-mode process, with different modes having random phases with respect to each other. As such, the detected *N*-photons may exist in different modes. This additional randomness further reduces the signal-to-noise seen in the interference fringes used for parameter estimation.

It was recently suggested that enclosing SPDC in a cavity may offer a solution to these issues [21]. The cavity doubles as a generator and a storage cavity of photons. Furthermore, operating in a cavity conveniently restricts the generated photons to a bandwidth-limited single transverse and longitudinal mode, which is ideal for many quantum applications [22]. In this paper, we present the results of a series of Monte Carlo simulations that examine the performance of such a proposal under realistic physical settings, and clearly establish its advantage, in comparison to an ordinary SPDC process with the same nonlinear interaction strength: 3dB photon-number squeezing in the cavity output which translates into an average 2-fold improvement in the probability of obtaining the desired photon Fock state; and more importantly, achieves that state up to 10 times faster.

2. Monte Carlo simulation

The proposed setup (Fig. 1) consists of a single cavity containing the nonlinear gain medium. The system operates in pulsed mode. At the beginning of a pump cycle, a pump pulse enters the cavity, drives the PDC process, and then exits the cavity. In a PDC process, the pump field excites a pair of daughter fields, i.e., for every pump photon consumed, two daughter photons are produced satisfying energy conservation $\omega_{\text{pump}} = \omega_{\text{a}} + \omega_{\text{b}}$ and momentum conservation $\vec{k}_{\text{pump}} = \vec{k}_{\text{a}} + \vec{k}_{\text{b}} + \vec{k}_{\text{G}}$, where $\vec{k}_{\text{G}}$ is a quasi-momentum accounting for periodic modulation of the crystal domain such as poling.

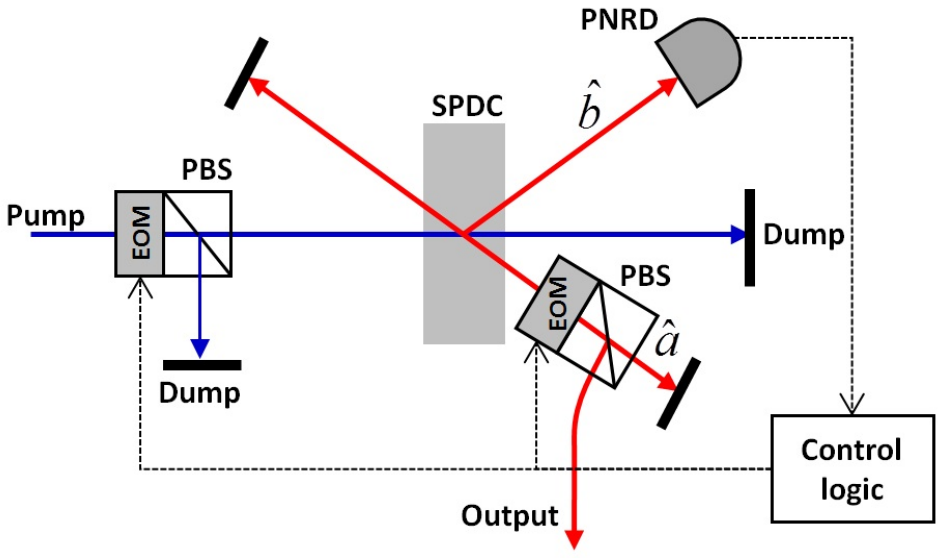

Fig. 1. Schematic of the proposed device. Mode $\hat{a}$ is the storage and accumulation mode. Mode $\hat{b}$ is the ancillary monitoring mode. The EOM-PBS in the pump path allows pump pulses to enter the cavity and modulates their power. The intra-cavity EOM-PBS releases the stored state upon reaching the goal number.

#206059 - $15.00 USD Received 28 Mar 2014; revised 29 May 2014; accepted 2 Jun 2014; published 15 Aug 2014

In our scheme, it is assumed that the modes $\hat{a}$ and $\hat{b}$ are non-degenerate in at least one degree of freedom (e.g., polarization), allowing for their separation. While mode $\hat{a}$ is stored (on resonance with the cavity), mode $\hat{b}$ immediately exits the cavity for PNR measurement (the ancillary number measurement). The number of photons detected in this measurement is reported as N_{new}, and added to the total N_{tot}. Mode $\hat{a}$ is circulated in synchronization with the next pump pulse to seed the PDC process, and is amplified by the next pump pulse. When N_{tot} reaches or exceeds N_{goal}, the photon number of desired Fock state, the stored state is released, e.g. by polarization rotation via an electro-optical modulator (EOM). In the following, we model this setup for a variety of settings and examine the statistics of the output states.

A single pump cycle can be described using a succession of three operators: gain, loss, and detection. The gain operator is $\hat{G}_{a,b} = \exp\left[\chi\left(\hat{a}^{\dagger}\hat{b}^{\dagger} - \hat{a}\hat{b}\right)\right]$. The loss is modeled with a unitary operator $\hat{U}_a = \exp\left[i\theta/2 \cdot \left(\hat{a}^{\dagger}\hat{c}^{\dagger} - \hat{a}\hat{c}\right)\right]$, with . Mode $\hat{c}$ represents the loss and is traced out. Coefficients t_a and r_a are transmission and reflection (loss) amplitudes, with $|t_a|^2 = |\cos(\theta/2)|^2$ and $|r_a|^2 = |\sin(\theta/2)|^2$. Mode $\hat{b}$ is treated similarly. The PNR detection of mode $\hat{b}$, represented by a set of positive-operator-valued-measurements (POVM), $\hat{\Pi}_b^{(m)} = \sum_{i=m}^{\infty} i\eta^m (1-\eta)^{i-m} |i\rangle_b \langle i|$ for detecting m-photons, with $\sum_{m=0}^{\infty} \hat{\Pi}_b^{(m)} = 1$ and $\hat{\Pi}_b^{(m)} \geq 0$, where η captures the loss of mode b in the travel and detection. Setting the initial input state to vacuum, the state reentering the process after the first pass is given as,

$$\rho_m = \mathrm{Tr}_c \left[\hat{U}_a^{+} \hat{G}_{a,b}^{+} \hat{U}_a \hat{\Pi}_b^{(m)} \hat{U}_a^{+} \hat{G}_{a,b}^{+} \hat{U}_a |0\rangle_{a,b} \langle 0| \right] |0\rangle_a \langle 0| \tag{1}$$

conditioned on an m-photon detection by the PNRD with the probability of,

$$P_b(m) = \mathrm{Tr}_a \left[\hat{G}_{a,b}^{+} \hat{\Pi}_b^{(m)} \hat{G}_{a,b} |0\rangle_{a,b} \langle 0| \right] \tag{2}$$

Equations (1) and (2) form the basis of our Monte Carlo simulation. During the measurement phase of each pump cycle, we derive a set of probabilities $\{P_b(m)\}$ for the corresponding states $\{\rho_m\}$ for all possible PNR detections of mode $\hat{b}$. As the input state for the next pump cycle, we choose a state randomly from $\{\rho_m\}$ based on the probability distribution of $\{P_b(m)\}$. The pump cycles continue until N_{tot}, the sum total of all photons detected in mode $\hat{b}$, reaches N_{goal}, the target photon number; then that particular trial is concluded. The final Fock state density distribution for mode $\hat{a}$ was converted into a probability distribution $P(N_{\text{ph}})$. A single simulation run consisted of 100 000 such trials. Individual probability distributions were then averaged together, producing $P_{\text{avg}}(N_{\text{ph}})$. Rate of success $P(N_{\text{goal}})$ and the standard deviation of photon numbers σ_{Nph} were calculated from $P_{\text{avg}}(N_{\text{ph}})$.

3. Simulation results and discussion

We first examined the amplification of a photon Fock state through the PDC process. Figure 2(a) shows the expected increased number of photons $\langle N_{\text{new}} \rangle$ in mode $\hat{b}$ (assuming no loss) immediately following a single pump cycle. Figure 2(b) shows the standard deviation

#206059 - $15.00 USD Received 28 Mar 2014; revised 29 May 2014; accepted 2 Jun 2014; published 15 Aug 2014

$\sigma(N_{\text{new}})$ for the same case. Figure 2(c) shows the expected number of pump cycles $\langle N_{\text{C}} \rangle$ needed to add one or more photons to mode $\hat{b}$. Cases for several values of amplification gain χ are presented. We note that increasing both the seeding number and the gain have the same effect: the new photons are created with fewer trials and in greater numbers. But while increasing the seeding number and gain increase the absolute uncertainty of the photon number, the mean added number $\langle N_{\text{new}} \rangle$ grows faster than $\sigma(N_{\text{new}})$, so the relative standard deviation of the added photon numbers actually decreases as the process progresses.

These observations suggest that starting with higher gain and ending with lower gain may increase the state delivery rate and reduce the photon-number uncertainty of the photon pulses output from the cavity. In addition to fixed-gain operation, we considered two adaptive gain strategies in the simulation – a fixed-risk strategy and a genetic algorithm optimization, both of which created a gain schedule, which consisted of gain values for each value of N_{tot}. Crystal's nonlinearity and focusing geometry were assumed fixed, so gain variation was achieved by varying the pump power. Separate gain schedules were generated for each N_{goal} and each cavity performance level. In the fixed-risk strategy, a risk factor P_{risk} defined as the probability of exceeding the N_{goal} was chosen. Then for each value of N_{tot} (for a given N_{goal}), a value of gain was chosen to satisfy the below condition:

$$P\left(N_{\text{new}} \geq N_{\text{goal}} - N_{\text{tot}}\right) \leq P_{\text{risk}} \tag{3}$$

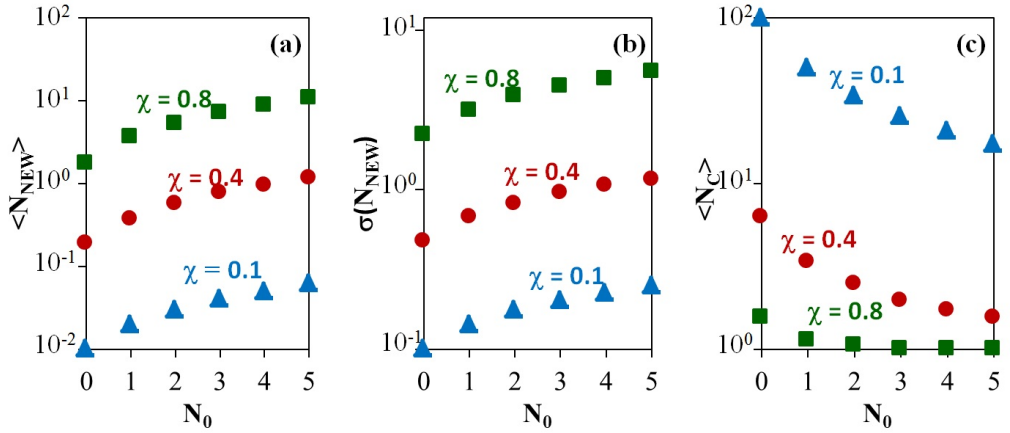

Fig. 2. Statistical properties of a state produced by seeding a PDC process of gain χ with a Fock state containing N_0 photons. (a) Expected number of new photons measured after a single pump cycle. (b) Standard deviation of the new photon numbers measured after a single pump cycle. (c) Expected number of pump cycles to have the first non-vacuum detection in mode $\hat{b}$.

During optimization, the value of P_{risk} was varied. For the strategy based on the genetic algorithm, it was the gain value for each N_{tot} value that was varied (except for $N_{\text{tot}} = 0$, in which case the gain was fixed at maximum, its value discussed below). For the case of fixed-gain operation, the value of the fixed gain was the optimization parameter. For all strategies, the value of $P(N_{\text{goal}})$ was maximized.

When comparing the two adaptive-gain strategies, it was found that while they produced nearly equivalent rates of success in terms of $P(N_{\text{goal}})$, the genetic algorithm provided a higher degree of squeezing in photon-number distribution. The adaptive-gain data discussed below was generated using the genetic algorithm optimization.

#206059 - $15.00 USD Received 28 Mar 2014; revised 29 May 2014; accepted 2 Jun 2014; published 15 Aug 2014

We studied cavity-PDC processes with N_{goal} varying from 4 to 12 for two different experimental conditions in the simulation: one labeled medium-performance ($T_{cav} = 95\%$, $\eta_{det} = 90\%$) and another labeled high-performance ($T_{cav} = 99\%$, $\eta_{det} = 95\%$). The range of χ was limited to less than 0.8. This limit corresponds approximately to the generation of on average 2 photon pairs in an SPDC process. This limit is based on the single-pass SPDC efficiency reported in [20], a 10 nJ pulse producing, on average, a single SPDC pair. A commercially available, non-amplified ultra-fast system can deliver approximately 20 nJ per pulse, therefore this was chosen as a reasonable limit on the pump power available in the simulation. Operation settings were individually optimized for each performance level and N_{goal} value. The simulation results shown in Figs. 3(a)–(c) are for high-performance and low-performance defined systems. The performance results are compared to three references: coherent light with a mean equal to N_{goal}, mean-equivalent thermal light, and power-equivalent thermal light. The power-equivalent thermal distribution is defined as the output resulting from a single-pass SPDC process pumped at maximum allowed power. Given the above SPDC efficiency approximation, this corresponds to a mean photon number of two.

Figure 3(a) shows that rate of success in all cases exceeded coherent and thermal light sources; fixed-gain and adaptive-gain strategies were similar, with a small advantage going to the adaptive gain. On average, the high-performance system improved on a coherent source's rate of success by a factor of 2.6, while the medium-performance provided an average improvement factor of 1.7.

Figure 3(b) shows that photon-number uncertainty was similar for the fixed- and adaptive-gain systems, but in all cases below the mean-equivalent Poisson distributions. On average, the high-performance system offered 3.2 dB (x2.1) of squeezing relative to a mean-equivalent Poisson source, while the medium-performance system provided 1.6 dB (x1.4) of squeezing.

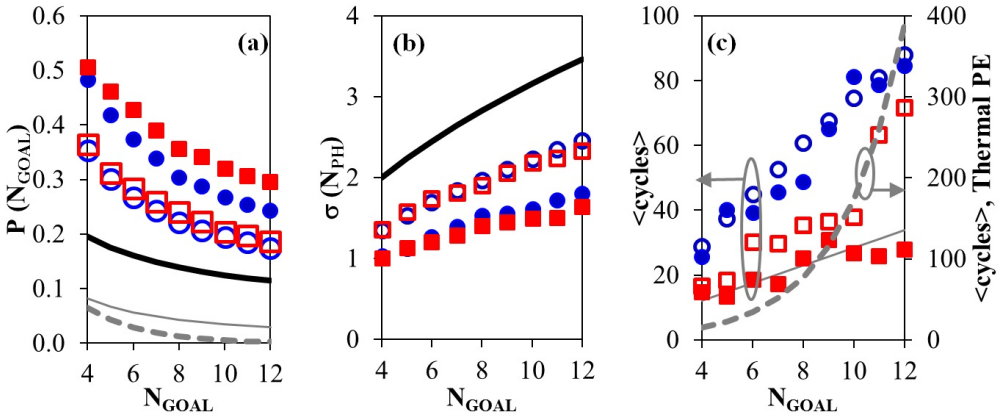

Fig. 3. Performance of the proposed scheme for a high-performance system (solid symbols), and a medium-performance system (open symbols). Fixed gain results (blue circles), and adaptive gain using genetic algorithm optimization (red squares). Shown for comparison: mean-equivalent Poisson distribution (black) and thermal distributions – mean-equivalent (solid grey) and power-equivalent (dashed grey). <cycles> is the expected number of pump cycles until N_{goal} is measured on the output using a perfect PNRD.

The main advantage of an adaptive-gain system can be seen in Fig. 3(c). On average, the adaptive-gain system delivered target states approximately twice as fast as a fixed-gain system. The rate of delivery was thus about equal to a mean-equivalent thermal distribution, and up to ten times faster than a power-equivalent thermally-distributed source.

#206059 - $15.00 USD Received 28 Mar 2014; revised 29 May 2014; accepted 2 Jun 2014; published 15 Aug 2014

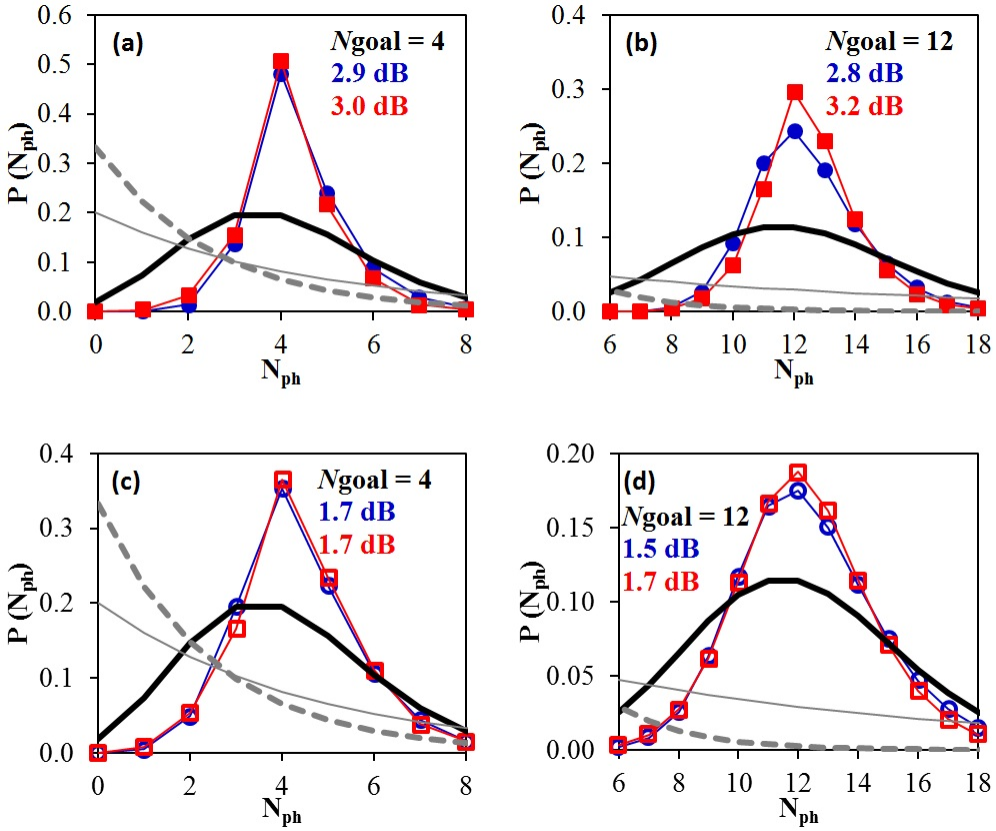

Fig. 4. Probability distribution produced by the proposed device. N_{goal} = 4, (a) high-performance and (c) medium-performance, and N_{goal} = 12, (b) high-performance and (d) medium-performance. Fixed-gain shown in blue and adaptive-gain in red. Included for comparison are what is possible with single-pass sources: shown are mean-equivalent Poisson distributions (black), thermal mean-equivalent (solid grey) and thermal power-equivalent (grey dashed) distributions.

An adaptive-gain system, on average, required 28 pump cycles to deliver a 12-photon state for the high-performance case, and 41 pump cycles for the medium-performance case. By comparison, a single-pass power-equivalent SPDC on average required 389 pump pulses to produce a 12-photon state.

Figure 4 shows the photon number distributions produced by the scheme with N_{goal} set to 4 or 12, exhibiting much reduced uncertainty compared to classical sources for both high and medium performance systems.

4. Conclusions

We have used Monte-Carlo simulation to examine a cavity-based PDC amplification process controlled by ancillary PNR measurements as a source of number squeezed states. The simulation included realistic system loss and detector efficiency, as well as typical pump power constraints. When targeting photon numbers in the range from 4 to 12, we observed 3 dB of squeezing with respect to mean-equivalent coherent states. The probability of generating the target number on the output state was 4 to 10 times greater than for a mean-equivalent thermal distribution. When taking into account the number of pump pulses expected to pass before the target number is achieved, the method presented was comparable to a mean-equivalent thermal distribution and significantly faster than a power-equivalent thermal source; the advantage grew for higher target numbers. We expect this approach, in

#206059 - $15.00 USD Received 28 Mar 2014; revised 29 May 2014; accepted 2 Jun 2014; published 15 Aug 2014

combining with other approaches, such as photon-multiplexing [23], may provide a significant and enabling technology in many quantum-enhanced schemes in such fields as metrology, communication, imaging, and sensing.

Acknowledgments

This research was supported in part by the Physics Frontier Center at Joint Quantum Institute. B. L. Glebov acknowledges the support of the Intelligence Community Postdoctoral Research Fellowship Program. All statements of fact, opinion, or analysis expressed are those of the author and do not reflect the official positions or views of the Intelligence Community or any other U.S. Government agency. Nothing in the contents should be construed as asserting or implying U.S. Government authentication of information or Intelligence Community endorsement of the author's views.

#206059 - $15.00 USD Received 28 Mar 2014; revised 29 May 2014; accepted 2 Jun 2014; published 15 Aug 2014